Competition between phase separation and spin density wave or charge density wave order: Role of long-range interactions

Bo Xiao, F. Hébert, G. Batrouni, and R. T. Scalettar

Competition between Phase Separation and Spin Density Wave or Charge Density Wave Order: The Role of Long-Range Interactions

Bo Xiao,[1] F. Hébert,[2] G. Batrouni,[2, 3, 4, 5, 6] and R.T. Scalettar[1]

[1]*Department of Physics, University of California, Davis, CA 95616,USA*
[2]*Université Côte d'Azur, CNRS, INPHYNI, France*
[3]*MajuLab, CNRS-UCA-SU-NUS-NTU International Joint Research Unit, 117542 Singapore*
[4]*Centre for Quantum Technologies, National University of Singapore, 2 Science Drive 3, 117542 Singapore*
[5]*Department of Physics, National University of Singapore, 2 Science Drive 3, 117542 Singapore*
[6]*Beijing Computational Science Research Center, Beijing 100193, China*
(Dated: May 13, 2019)

Recent studies of pairing and charge order in materials such as FeSe, SrTiO$_3$, and 2H-NbSe$_2$ have suggested that momentum dependence of the electron-phonon coupling plays an important role in their properties. Initial attempts to study Hamiltonians which either do not include or else truncate the range of Coulomb repulsion have noted that the resulting spatial non-locality of the electron-phonon interaction leads to a dominant tendency to phase separation. Here we present Quantum Monte Carlo results for such models in which we incorporate both on-site and intersite electron-electron interactions. We show that these can stabilize phases in which the density is homogeneous and determine the associated phase boundaries. As a consequence, the physics of momentum dependent electron-phonon coupling can be determined outside of the trivial phase separated regime.

I. 1. INTRODUCTION

The challenging nature of the computational solution of the quantum many electron problem has led, to a quite considerable extent, to consideration of models which incorporate only a single type of interaction. For example, the Hubbard and periodic Anderson Hamiltonians focus on on-site electron-electron repulsion, the Kondo model on an interaction with local spin degrees of freedom, while the Holstein and Su-Schrieffer-Heeger Hamiltonians consider exclusively electron-phonon interactions. This is, of course, an unfortunate situation, since the interplay between different interactions can lead to transitions between associated ordered phases which are of great interest. Even more importantly, this competition is present in most real materials. Quantum Monte Carlo (QMC) simulations of the Hubbard-Holstein Hamiltonian in two dimensions[1–9] have reinforced the challenges of, as well as the interest in, including multiple interactions. A very recent study offers great promise in developing a QMC approach in which electron-electron and electron-phonon interactions can be folded together, at least in the particular region of the phase diagram where charge order dominates[10].

One dimensional systems have offered an exception to this rule, largely because specialized algorithms exist in cases when the restricted geometry forbids the exchange of electrons[11]. Thus the extended Hubbard model (EHH), which includes electron-electron interactions in the form of both an on-site U and an intersite V is now known to include not only the expected charge density wave (CDW) correlations for $U < 2V$ and spin density wave (SDW) correlations (for $U > 2V$), but also a subtle bond ordered wave (BOW) phase in a narrow region about the line $U = 2V$[12–19]. These simulations have been used to understand better the behavior of different materials, including organic superconductors[21], density wave materials[22], and undoped conducting polymers[20]. Even with the applicability of these one-dimensional approaches, however, the physics remains subtle, and even controversial, owing mainly to energy gaps vanishing exponentially in the limit of weak coupling.

The goal of the present paper is an investigation of the physics of a Hamiltonian which includes long range electron-phonon coupling as well as electron-electron interactions U and V. Motivation is given by several recent situations in which momentum-dependent electron-phonon coupling (which necessitates non-local coupling in real space) has been suggested to be important, as we discuss below. Our work builds on the considerable earlier literature of one dimensional models with mixed interactions, which we review. As a first step, we focus here on half-filling and the effects of coexistence of long range electron-phonon coupling and electron-electron interactions. However, our numerical method, introduced in the following section, can be applied to this model at any fillings without a sign problem.

A further reason to focus on longer range interactions is in the search for one dimensional models which exhibit superconductivity as their dominant correlation. Despite an initial suggestion to the contrary[23], it now seems most likely that the one dimensional Hubbard-Holstein model with only on-site electron-phonon coupling, does not have dominant pairing fluctuations[24,25]. Instead, an 'extended Holstein' model, in which phonons residing on the midpoints between lattice sites couple to the

electronic charge both to the left and to the right, has been put forth as a 'minimal model' in which the electron-phonon can dominate over the more typical gapped CDW and SDW phases at half-filling[26,27].

We begin by writing down the full Hamiltonian, and then consider the various limiting cases before investigating the physics when all terms are present. Our model is,

$$\hat{\mathcal{H}} = \hat{\mathcal{K}} + \hat{\mathcal{H}}_{ph} + \hat{\mathcal{P}}_u + \hat{\mathcal{P}}_v + \hat{\mathcal{P}}_{ep}$$

$$\hat{\mathcal{K}} = -t \sum_{l,\sigma} \left(\hat{c}^{\dagger}_{l,\sigma} \hat{c}_{l+1,\,\sigma} + \hat{c}^{\dagger}_{l+1,\,\sigma} \hat{c}_{l,\sigma} \right)$$

$$\hat{\mathcal{H}}_{ph} = \frac{1}{2} \sum_l \left(\omega^2 \hat{X}_l^2 + \hat{P}_l^2 \right)$$

$$\hat{\mathcal{P}}_u = U \sum_l \hat{n}_{l,\uparrow} \hat{n}_{l,\downarrow}$$

$$\hat{\mathcal{P}}_v = V \sum_l \left(\hat{n}_{l,\uparrow} + \hat{n}_{l,\downarrow} \right) \left(\hat{n}_{l+1,\uparrow} + \hat{n}_{l+1,\downarrow} \right)$$

$$\hat{\mathcal{P}}_{ep} = \sum_{l,r} \lambda(r) \hat{X}_l \left(\hat{n}_{l+r,\uparrow} + \hat{n}_{l+r,\downarrow} \right) \tag{1}$$

Here $\hat{\mathcal{H}}$ is comprised of a kinetic energy ($\hat{\mathcal{K}}$) describing the hopping of fermions along a one-dimensional chain of N sites; an on-site repulsion U between fermions of opposite spin σ ($\hat{\mathcal{P}}_u$); an intersite repulsion V between fermions on adjacent sites ($\hat{\mathcal{P}}_v$); and, finally, an electron-phonon coupling ($\hat{\mathcal{P}}_{ep}$). All energies will be measured in units of $t = 1$. We choose the Fröhlich form,

$$\lambda(r) = \frac{\lambda_0 \, e^{-r/\xi}}{(1+r^2)^{3/2}} \ , \tag{2}$$

which modulates the long-range interaction between electrons and phonons with a screening length ξ (measured in units of the lattice constant $a = 1$). In the $\xi \to 0$ limit, the local electron-phonon coupling of the Holstein model is recovered. In the $\xi \to \infty$ limit, the interaction is reduced to a lattice version of Fröhlich model. Throughout this paper we will consider the half-filled situation where $\rho = (N_{\uparrow} + N_{\downarrow})/N = 1$ with N_{σ} the numbers of electrons of spin σ. Although we are generalizing the range of the electron-phonon interaction from the $\xi = 0$ Holstein limit, we will continue to consider only local phonon degrees of freedom, i.e. neglecting intersite interactions between the phonons which would give rise to dispersive phonon modes[28].

The ('pure') Hubbard Hamiltonian (HH) $\hat{\mathcal{K}} + \hat{\mathcal{P}}_u$ is exactly soluble in 1D via the Bethe *ansatz*[29]. For all non-zero values of U, the ground state has spin order, with power law decaying spin-spin correlations. The Bethe *ansatz* solution already interjects a cautionary note for numerical work: the gap which immediately opens for $U > 0$ is exponentially small.

The physics of the ground state of the extended Hubbard Hamiltonian (EHH) $\hat{\mathcal{K}} + \hat{\mathcal{P}}_u + \hat{\mathcal{P}}_v$ has already been noted above: CDW with true long range order

(owing to the discrete symmetry of the order parameter) dominates for $U < 2V$, with weaker, power law decaying SDW correlations at $U > 2V$ when the symmetry is continuous. The BOW phase consists of a pattern in which the hopping $\hat{c}^{\dagger}_{l,\sigma} \hat{c}_{l+1,\,\sigma} + \hat{c}^{\dagger}_{l+1,\,\sigma} \hat{c}_{l,\sigma}$ serves as a staggered order parameter, alternating in amplitude for l odd and even. As for the CDW phase, the discrete nature of the breaking of the translational symmetry in the BOW gives true long range order[12].

The Holstein Hamiltonian $\hat{\mathcal{K}} + \hat{\mathcal{H}}_{ph} + \hat{\mathcal{P}}_{ep}$ neglects the electron-electron interaction terms, and also sets $\xi = 0$ so that only the on-site piece of $\hat{\mathcal{P}}_{ep}$ survives. Similar to the HH, an (exponentially small) gap opens immediately for any $\lambda_0 > 0$ for small phonon frequencies. The existence of a gap for large ω is still controversial, despite an impressively large set of numerical and analytic investigations[30–39].

The Holstein extended Hubbard (HEH) Hamiltonian includes all the terms $\hat{\mathcal{K}} + \hat{\mathcal{H}}_{ph} + \hat{\mathcal{P}}_u + \hat{\mathcal{P}}_v + \hat{\mathcal{P}}_{ep}$, again setting $\xi = 0$. The key added feature here is the possible existence of a gapless metallic phase. This occurs when the effective electron-electron attraction $U_{\text{eff}} = -\lambda_0^2/\omega^2$ mediated by integrating out the phonons, balances the on-site repulsion U. Contradictory results concerning this gapless phase exist[23,24,35,38,40–46].

Finally, some work has been done on extensions of the HEH which allow for non-local electron-phonon coupling. As noted earlier, Bonca and Trugman[26] and later Tam *et al.*[27] considered a situation in which a phonon mode exists on the bond between two sites, coupling to the sum of the fermionic density on the two endpoints. This work was based on the observation that, for the commensurate densities under consideration here, diagonal long range orders, *i.e.* SDW and CDW, almost invariably dominate over superconductivity. The bond phonon mode will clearly favor the formation of pairs on adjacent sites, opening the door to the possibility of off-diagonal long range order. Indeed, singlet superconductivity was shown to occur in the small U, V portion of the phase diagram.

Motivated by the observation that the long-range electron-phonon interaction supports light polaron and bipolaron physics observed in the cuprates, Hohenadler *et al.*[49] simulated the fermion-boson model with the Fröhlich interaction. They found that the extended interactions suppress the Peierls instability and balance CDW and s-wave pairing. With similar motivation, for fullerenes and manganites, Spencer *et al.*[48] studied the ground state properties of the screened Fröhlich polaron in weak, strong and intermediate coupling regions, as well various screening lengths.

Following this review, we conclude this introduction with the background and motivation for investigation of the full HEH with the Fröhlich form of the electron-phonon coupling (Eq. 1). In the dilute limit, continuous-time quantum Monte Carlo (CTQMC) has been used to study the effect of varying the range ξ on polaron and bipolaron formation[50]. The interest in studying

general momentum-dependent coupling constants is driven by a number of factors. First, a momentum dependent $\lambda(q)$ is implicated in several experimental situations of considerable current interest, including the origin of the ten-fold increase in the SC T_c of FeSe monolayers[51], the disparity in the values of the electron-phonon coupling in SrTiO$_3$ inferred from tunneling below T_c and angle-resolved photoemission (ARPES) in the normal state[52], and the "extended phonon collapse" in 2H-NbSe$_2$[54]. Second, there are qualitative issues to be addressed, e.g. how the range of the electron phonon interaction ξ affects the competition between metallic and Peierls/CDW phases at half-filling. Here recent CTQMC studies in one dimension have shown that as ξ increases from zero, the metallic phase is stabilized and, for sufficiently large λ, phase separation (PS) can also occur[49]. Finally, it has been argued that recent improvements in the energy resolution of resonant inelastic x-ray scattering (RIXS) have opened the possibility of an experimental determination of the electron-phonon coupling across the full Brillouin zone[55]. This observation carries the exciting implication that materials-specific forms for $\lambda(q)$, can be incorporated into QMC simulations of appropriate model Hamiltonians.

Unfortunately, one cannot immediately study the simple case of a longer range electron-phonon interaction in isolation. The reason is that when a fermion distorts the lattice for ξ finite, it does so at a collection of sites in its vicinity. This distortion attracts additional fermions, further increasing the distortion. The resulting cascade leads to a very high tendency to phase separation. The Holstein Hamiltonian ($\xi = 0$) neatly evades this collapse since the Pauli principle caps the fermion count on a displaced site. Likewise, the Bonca and Trugman model of bond phonons restricts the electron-phonon coupling to a pair of sites. The solution to this dilemma in the general case is clear- the inclusion of non-zero electron-electron repulsion. A recent study which incorporates on-site U but retains $V = 0$[53] revealed continued phase separation over much of the phase diagram, with SDW occurring only if ξ and λ_0 were rather small. We show here that V can significantly stabilize the CDW and SDW phases against collapse of the density.

II. 2. COMPUTATIONAL METHODOLOGY

Our technical approach is a straightforward generalization of the world-line quantum Monte Carlo (WLQMC) method for lattice fermions of Hirsch et al.[11]. In this method, a path integral is written for the partition function by discretizing the inverse temperature β into intervals of length $\Delta\tau = \beta/L$.

$$
\begin{aligned}
\mathcal{Z} &= \mathrm{Tr}\big[\,e^{-\beta\hat{\mathcal{H}}}\,\big] \\
&= \mathrm{Tr}\big[\,e^{-\Delta\tau\hat{\mathcal{H}}_1}\,e^{-\Delta\tau\hat{\mathcal{H}}_2}\cdots e^{-\Delta\tau\hat{\mathcal{H}}_1}\,e^{-\Delta\tau\hat{\mathcal{H}}_2}\,\big]
\end{aligned}
\tag{3}
$$

On the odd imaginary time intervals, half of the Hamiltonian of Eq. 1 acts,

$$
\begin{aligned}
\hat{\mathcal{H}}_1 &= \hat{\mathcal{K}}_1 + \frac{1}{2}\big(\hat{\mathcal{H}}_{ph} + \hat{\mathcal{P}}_u + \hat{\mathcal{P}}_v + \hat{\mathcal{P}}_{ep}\big) \\
\hat{\mathcal{K}}_1 &= -t\sum_{l\in\mathrm{odd},\,\sigma}\big(\hat{c}_{l,\sigma}^{\dagger}\hat{c}_{l+1,\,\sigma} + \hat{c}_{l+1,\,\sigma}^{\dagger}\hat{c}_{l,\sigma}\big)
\end{aligned}
\tag{4}
$$

while on the even intervals the other half acts,

$$
\begin{aligned}
\hat{\mathcal{H}}_2 &= \hat{\mathcal{K}}_2 + \frac{1}{2}\big(\hat{\mathcal{H}}_{ph} + \hat{\mathcal{P}}_u + \hat{\mathcal{P}}_v + \hat{\mathcal{P}}_{ep}\big) \\
\hat{\mathcal{K}}_2 &= -t\sum_{l\in\mathrm{even},\,\sigma}\big(\hat{c}_{l,\sigma}^{\dagger}\hat{c}_{l+1,\,\sigma} + \hat{c}_{l+1,\,\sigma}^{\dagger}\hat{c}_{l,\sigma}\big)
\end{aligned}
\tag{5}
$$

The division of $\hat{\mathcal{H}}$ into two pieces necessitates the presence of $2L$ time slices.

Complete sets of occupation number and phonon coordinate states are inserted between each incremental time evolution operator. The matrix elements are then evaluated, replacing all operators by space and imaginary time dependent c-numbers corresponding to the eigenvalues of the intermediate states. The fermion occupation number states and phonon coordinate states are sampled stochastically by introducing local changes and accepting/rejecting according to the ratio of matrix elements.

The utility of the "checkerboard decomposition"[11] is that on each imaginary time slice the matrix element of the incremental time evolution operator factorizes into a product of independent two site problems. The matrix elements are thus simple to evaluate. The Monte Carlo moves are chosen to preserve local conservation laws of the particle count on each two site plaquette.

The strengths of the WLQMC approach include a linear scaling in spatial system size N and imaginary time β (in contrast to the N^3 scaling of auxiliary field QMC). This is a consequence of the locality of the values of the matrix elements. More significantly, there is no fermion sign problem[56,57] at any filling as long as the hopping occurs exclusively between sites which are adjacent in the list of occupation numbers labeling the state.

In this work we will be interested in the ground state properties of Eq. 1, which we access by choosing β sufficiently large. Our typical choice is $\beta \sim N$. We have checked that we have reached the low T limit, with the caveat noted earlier that the exponential scaling of the gap precludes this at weak coupling. In what follows, we note when that concern affects our conclusions significantly.

The realization Eqs. 3-5 of WLQMC works in the canonical ensemble, although it is straightforward to connect to grand-canonical ensemble results by doing simulations on adjacent particle number sectors and extracting the chemical potential from a finite difference of ground state energies of systems of different particle number[58].

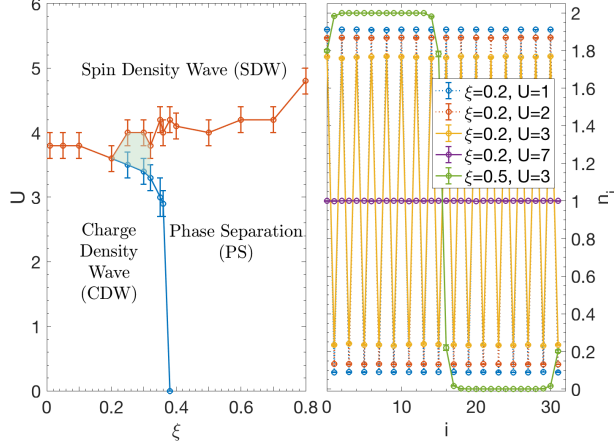There are some weaknesses to the method. Most notably, it is challenging to evaluate expectation values

FIG. 1. (Color online) (a) Phase diagram of the HEH in the U-ξ plane at fixed $V = 0$ and $\omega = 0.5, \lambda_0 = 1.0$. The lattice size is $N = 32$ and inverse temperature $\beta = 26$. The procedure for determining the positions of the phase boundaries is described in subsequent figures and discussion, and in the right-hand panel. (b) Snapshots of electron density $(n_i = n_{i,\uparrow} + n_{i,\downarrow})$ profiles. For $\xi = 0.5, U = 3$, the particles are clumped in one region of the lattice- the system exhibits PS. For $\xi = 0.2, U = 7$, the total density is uniform, as expected for an SDW where spin density oscillates, but charge density is constant. The three data sets at $\xi = 0.2$ with $U = 1, 2, 3$ are in the CDW phase. The order parameter (size of charge oscillation) decreases as U grows and the phase boundary to the SDW is approached.

of operators which 'break' the world lines. Thus access to single and two particle Green function is restricted, unlike other methods like the 'worm'[59] and stochastic Green function (SGF)[60] approaches. In addition, WLQMC often suffers from long autocorrelation times which are associated with the local nature of the moves, and the tendency for world lines to have significantly extended spatial patterns. Both of these are addressed in the worm and SGF methods, at, however, the cost of somewhat greater algorithmic complexity. Here, in $d = 1$ due to the speed of the approach, one can tolerate long autocorrelations simply by doing many updates.

In order to determine the phase diagram of Eq. 1, we monitor first a set of local observables: the fermion kinetic energy, phonon kinetic energy, and fermion double occupancy,

$$\mathcal{K}_{el} = -t \left\langle \left(\hat{c}^\dagger_{l,\sigma} \hat{c}_{l+1,\sigma} + \hat{c}^\dagger_{l+1,\sigma} \hat{c}_{l,\sigma} \right) \right\rangle$$
$$\mathcal{K}_{ph} = \frac{1}{2} \left\langle \hat{P}_l^2 \right\rangle$$
$$\mathcal{D} = \left\langle \hat{n}_{l,\uparrow} \hat{n}_{l,\downarrow} \right\rangle \tag{6}$$

In the absence of a broken CDW or BOW symmetry, these are independent of lattice site l since $\mathcal{H}$ is translation invariant. Second, we evaluate the CDW and

SDW structure factors,

$$S_{cdw} = \frac{1}{N} \sum_{l,j} \left\langle \left(\hat{n}_{l,\uparrow} + \hat{n}_{l,\downarrow} \right) \left(\hat{n}_{j,\uparrow} + \hat{n}_{j,\downarrow} \right) \right\rangle (-1)^{j+l}$$
$$S_{sdw} = \frac{1}{N} \sum_{l,j} \left\langle \left(\hat{n}_{l,\uparrow} - \hat{n}_{l,\downarrow} \right) \left(\hat{n}_{j,\uparrow} - \hat{n}_{j,\downarrow} \right) \right\rangle (-1)^{j+l} \tag{7}$$

to get insight into long range order (LRO). These structure factors are independent of N in a disordered phase, but grow with N in an ordered or quasi-ordered phase, as the associated real space correlation functions remain non-zero at large separations $|j - l|$. Although the quantities of Eq. 6 are local and hence in principle not appropriate to determining the appearance of non-analyticities associated with transitions, we shall see that they nevertheless show sharp signatures at the phase boundaries.

We also investigate the non-local observables including the charge and spin susceptibilities which involve an additional integration over imaginary time,

$$\chi_{charge} = \frac{\Delta\tau}{N} \sum_{\tau,l,j} \left\langle \hat{n}_l(\tau) \hat{n}_l(0) \right\rangle (-1)^{j+l}$$
$$\hat{n}_l(\tau) = \left(\hat{n}_{l,\uparrow} + \hat{n}_{l,\downarrow} \right)(\tau)$$
$$= e^{\tau\hat{\mathcal{H}}} \left(\hat{n}_{l,\uparrow} + \hat{n}_{l,\downarrow} \right)(0) e^{-\tau\hat{\mathcal{H}}}$$
$$\chi_{spin} = \frac{\Delta\tau}{N} \sum_{\tau,l,j} \left\langle \hat{m}_l(\tau) \hat{m}_l(0) \right\rangle (-1)^{j+l}$$
$$\hat{m}_l(\tau) = \left(\hat{n}_{l,\uparrow} - \hat{n}_{l,\downarrow} \right)(\tau)$$
$$= e^{\tau\hat{\mathcal{H}}} \left(\hat{n}_{l,\uparrow} - \hat{n}_{l,\downarrow} \right)(0) e^{-\tau\hat{\mathcal{H}}} \tag{8}$$

The susceptibility provides a clearer signal of the SDW transition, which is more subtle than the CDW transition owing to the continuous nature of the symmetry involved.

III.   3. PHASE DIAGRAMS AT FIXED V

In this section we present the phase diagrams in the U-ξ plane at three fixed values of intersite electron-electron repulsion V, focussing on the stabilization of the ordered phases by V against phase separation. We begin by showing, in Fig. 1(a), the phase diagram for vanishing intersite repulsion $V = 0$ and with $\omega = 0.5, \lambda_0 = 1.0$. CDW correlations, driven solely by the electron-phonon interaction (since $V = 0$), dominate at small U and ξ, but are replaced by SDW as U increases, or by PS as ξ increases. Figure 1(a) emphasizes the fragility of CDW order to PS: an electron-phonon interaction range as short as a few tenths of a lattice spacing is sufficient to drive the system into a regime where all electrons clump together. Although the errors bars make it somewhat uncertain, the data in the range $0.2 \leq \xi \leq 0.35$ indicate
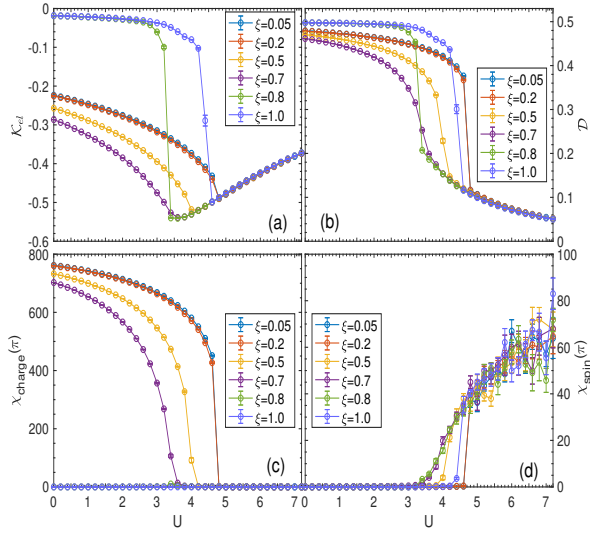
FIG. 2. (Color online) (a) Electron kinetic energy as a function of on-site repulsion U for fixed intersite repulsion, $V = 0.5$, and different values of electron-phonon interaction screening length ξ. (b) Double occupancy as a function of U. A sharp drop in $\mathcal{D}$ and a sharp increase in the magnitude of $\mathcal{K}_{el}$ remark the entry into the SDW phase from the large ξ PS region as U increases. Structure at smaller ξ is associated with the CDW-SDW boundary (See text and Fig. 3(a)). (c) Charge susceptibility as a function of U. χ_{charge} is big in the weak U CDW phase, and drops at the SDW boundary. (d) The spin susceptibility shows the opposite trend: χ_{spin} is small at weak U, but increases as the SDW phase is entered at large U. The lattice size is $N = 32$ and inverse temperature $\beta = 26$. The phonon frequency is fixed at $\omega = 0.5$ and electron-phonon coupling strength $\lambda = 1.0$.

the possibility of penetration of a thin PS wedge at the SDW-CDW boundary.

Figure 1(b) provides direct visualization of total electron density on each lattice site. The alternating pattern in the CDW phase region reflects true long range charge order in the ground state. Quantum fluctuations due to the hopping t reduce the magnitudes of the largest and the smallest densities from perfect double occupation $(n_i = 2)$ and empty $(n_i = 0)$. For fixed screening length $\xi = 0.2$, Fig. 1(b) shows the CDW phase is most stable at small U, with the charge oscillations decreasing in size as U grows, ultimately vanishing at $U = 7$ in the SDW. The figure also displays a subtle difference in the double occupancy $\mathcal{D}$ between the CDW and PS regions. Both have half their sites nearly empty and half nearly doubly occupied, but in the CDW case the n_i values are farther from their extreme limits $n_i = 0, 2$. The reason is that the alternation of empty and doubly occupied sites in the CDW allows for a much greater degree of quantum fluctuations due to the hopping t than can occur in the PS state where the Pauli principle blocks fermion mobility.

As noted in the introduction, mitigating the strong tendency to PS at $V = 0$ is what that motivates our work here. The results of Fig. 1 are consistent with those

obtained at $V = 0$ in Ref.[53], which uses the alternate stochastic Green function[60] method.

We now turn to non-zero V. Our discussion will detail how Fig. 1, and subsequent phase diagrams, are obtained through the analysis of the evolution of the observables of Eqs. 6-8.

Figure 2(a) shows the kinetic energy of the electrons, $\mathcal{K}_{el}$, for a range of values of ξ as a function of the on-site U for fixed $V = 0.5, \omega = 0.5$, and $\lambda_0 = 1.0$. For $\xi \gtrsim 0.8$, $\mathcal{K}_{el}$ is small until U exceeds a critical value. This change is associated with a transition from a small U PS state, where the clumped electrons are unable to move (except at the boundary of the occupied region) due to Pauli blocking, to a large U SDW state where alternating up and down occupation allows considerable intersite hopping and hence large (in magnitude) $\mathcal{K}_{el}$. See Fig. 3(a). At strong U we expect the hopping to go as t^2/U (second order perturbation induced by virtual hopping), and indeed this fall-off fits the large U data reasonably well. The value of the on-site repulsion U which is needed to eliminate PS is reduced as ξ is lowered, as is expected since the tendency for particles to clump is reduced as their interaction range is shortened.

In the small ξ (Holstein) limit PS does not occur. Nevertheless $\mathcal{K}_{el}$ and $\mathcal{D}$ show appropriate signals of the CDW-SDW transition: $\mathcal{K}_{el}$ is largest in magnitude at the boundary where the two insulators most closely compete, and $\mathcal{D}$ becomes small as the SDW is entered. The more rounded feature of $\mathcal{K}_{el}$ at intermediate ξ is one indication of the possible intrusion of PS between CDW and SDW. Again, see Fig. 3(a).

The double occupancy $\mathcal{D}$ is given in Fig.2(b). To interpret it, we first note that $\mathcal{D}$ is not a good discriminator between PS and CDW, because, in both, one has (subject to quantum fluctuations) roughly half the sites doubly-occupied and half empty, and hence $\mathcal{D} \sim 0.5$. In the SDW phase, on the other hand, $\mathcal{D} \sim 0$ since U precludes double occupancy. Thus the most evident feature of Fig.2(b) is the sharp drop in $\mathcal{D}$ as U increases which occurs for all ξ. These occur at values consistent with the increase in the magnitude of $\mathcal{K}_{el}$ of Fig.2(a). $\mathcal{D}$ is not strictly zero in the SDW phase because of the quantum (charge) fluctuations induced by t. These gradually go down at U increases.

Despite the fact that $\mathcal{D} \sim 0.5$ in both the CDW and PS states, Fig. 2(b) still shows a subtle signature of the CDW-PS transition with increasing ξ at fixed U: $\mathcal{D}$ initially falls as ξ increases from $\xi = 0.2$ to $\xi = 0.7$, but then rises again from $\xi = 0.7$ to $\xi = 1.0$. The somewhat smaller values of $\mathcal{D}$ in the CDW result from fluctuations which are morely likely when doubly occupied sites are surrounded by empty sites than in the PS state where they are adjacent to each other. This signal of the CDW-PS boundary of Fig. 3(a), although weak, is quite clear, and lines up well with the small U features in $\mathcal{K}_{el}$ in Fig. 2(a).

The spin susceptibility in Fig. 2(d) reinforces the inferences made from the local observables and confirms

the large U phase is SDW. For each value of ξ, a sharp increase in χ_{spin} occurs as U increases. The critical value is not very sensitive to ξ, changing from $U_c \sim 4.8$ at $\xi \sim 0.2$ to $U_c \sim 4$ at $\xi \sim 0.8$. This is reflected in the nearly horizontal character of the phase boundary of Fig. 3(a). In the complete absence of any thermal or quantum fluctuations we have $\chi_{\text{spin}} = N\beta$ from Eq. 8. The values of Fig. 2(d) are an order of magnitude smaller: Quantum fluctuation reduce correlations significantly, especially in one dimension and for the case of a continuous order parameter which has power law correlations at $T = 0$.

Finally, the charge susceptibility is shown in Fig. 2(c). For $\xi \lesssim 0.7$, χ_{charge} is large at small U, indicating the presence of CDW order until PS and then SDW occur as U increases. For larger ξ there is no small U CDW phase. These observations are consistent with the measurement of the local observables and spin susceptibility of Figs. 2(a), Figs. 2(b) and 2(d).

The full phase diagram at $V = 0.5$ is given in Fig. 3(a). The PS regime has been pushed out to $\xi \sim 0.8$, in contrast to $\xi \sim 0.38$ in Fig. 1(a). The SDW phase boundary is remarkably flat: $U_c \sim 4 - 5$ regardless of the nature of the phase (CDW or PS) beneath it. For small ξ the CDW region is also increased in size vertically upward in going from $V = 0$ to $V = 0.5$. This upward shift has been discussed by Hirsch[30] in the Holstein limit of local electron-phonon interaction: Nonzero V combines with the tendency to form CDW order driven by the electron-phonon interaction, producing a $2V$ change in the position of the CDW-SDW boundary. This estimate is in good quantitative agreement with what we find in comparing Figs. 1(a) and 3(a). In Fig. 3(b) and Fig. 3(c), we show the finite size effects on the normalized charge structure factor $S_{\text{charge}}(\pi)/N$ and $\mathcal{K}_{el}$ at $\xi = 0.1$. We have verified that the finite size effects for this parameter set are typical of those throughout phase space, allowing us to locate the phase boundaries accurately.

Just as the precise nature of the boundary between CDW and SDW in the extended Hubbard model was challenging to uncover, with the original picture of a direct transition (with a change from first to second order at at tricritical point) being replaced by an intervening BOW[12], in our studies the nature of a narrow region where the CDW-SDW boundary meets PS is ambiguous. The technical issue is the difficulty in locating the precise positions of the CDW and SDW transitions given the rounding effects of finite size lattices. We have indicated this uncertainty, which is greater as we turn on V, by a shaded region in Fig. 3(a).

We will not show the detailed evolution of observables for larger $V = 1$, since their basic structure is the same as for $V = 0.5$, just discussed. Figure 4 is the resulting phase diagram. PS has been pushed to the region $\xi \gtrsim 1.2$. For smaller ξ, while PS is absent, the increasing range of the el-ph coupling tilts the CDW-SDW in favor of spin order. In the Holstein limit, $\xi = 0$, the electron-phonon and nearest neighbor electron-electron interactions work in concert to promote charge order. It is clear that as ξ
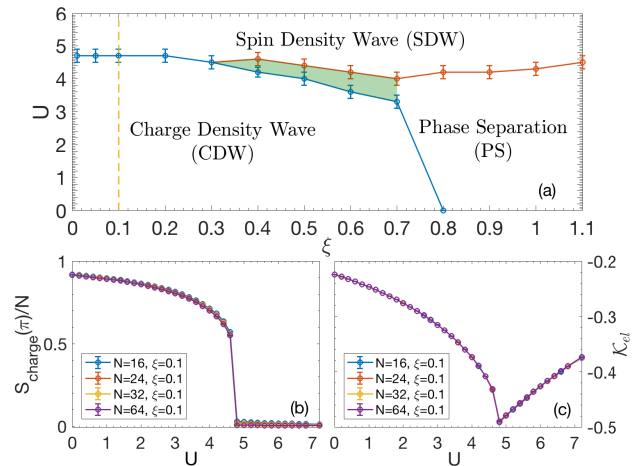

FIG. 3. (Color online) (a)Phase diagram of the HEH model in the U-ξ plane for $V = 0.5$. Compared to Fig. 1(a) the CDW-PS line is pushed out from $\xi \approx 0.38$ at $V = 0$ to $\xi \approx 0.8$ here. In the Holstein limit, CDW correlations are stabilized by an amount $2V$ against SDW. The uncertainty in the precise nature of the phase where the CDW, SDW, and PS regions meet is indicated by the shaded region. See text. (b)Finite size effect on the normalized charge structure factor $S_{\text{charge}}(\pi)/N$ at $\xi = 0.1$. The magnitude of $S_{\text{charge}}(\pi)$ is proportional to the size of lattice, indicating the existence of true long-range order in the CDW phase. Therefore, the normalized charge structure factor $S_{\text{charge}}(\pi)/N$ is N independent in the CDW phase. $S_{\text{charge}}(\pi)/N$ changes abruptly at the same U/t value for all N. (c) Electron kinetic energy $\mathcal{K}_{el}$ (per site) for different lattice sizes at $\xi = 0.1$. The position of the cusp is N independent.

increases the electron-phonon interaction no longer favors double occupation on the same site over occupation of adjacent sites, leading to the downward slope of the CDW boundary.

One might expect that as $\xi \to \infty$, the electron-phonon interaction becomes independent of the fermion positions, and hence that the CDW-SDW boundary should approach the usual $U = 2V$ position. The CDW boundary is indeed decreasing as ξ grows, but for $V = 1$ phase separation still occurs before the $V = 2U$ values. For large ξ, the fact that the boundary of phase transition from CDW or PS state to SDW state decreases compared to the Holstein limit suggests that the effective attraction, U_{eff}, is smaller in Fröhlich model than in Holstein model.

IV. 4. PHASE DIAGRAMS AT FIXED U

We now show a set of complementary phase diagrams in the $V - \xi$ plane at fixed U. Since their derivation lies in the same detailed analysis of χ_{charge}, χ_{spin}, as well as $\mathcal{K}_{el}$ and $\mathcal{D}$, to that of the preceding section, we focus mostly on the final phase diagrams.
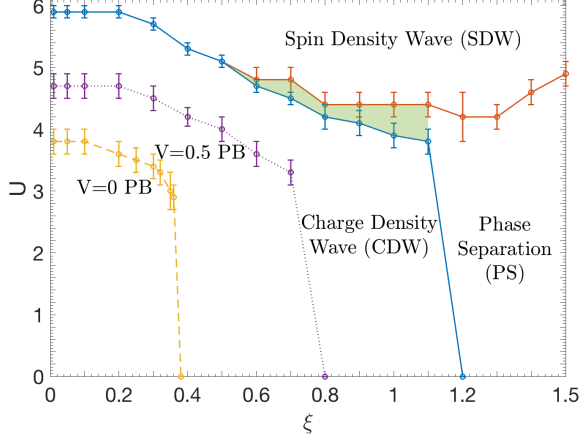
We consider first small ($U = 3$) and large ($U = 8$)

FIG. 4. (Color online) Phase diagram of the HEH model in the U-ξ plane for $V = 1.0$ (solid lines). The dashed and dotted lines indicate the phase boundary (PB) of the CDW region $V = 0$ and $V = 0.5$, with the SDW boundaries of Figs. 1(a) and 3(a) suppressed for clarity. As the intersite V increases, the charge density wave is stabilized to longer range electron-phonon interaction range ξ. At $\xi = 0$ the CDW-SDW phase boundary moves upward approximately by $2V$[30]. As with the preceding figure, the uncertainty in the precise nature of the phase where the CDW, SDW, and PS regions meet is indicated by the shaded region.

on-site repulsion, which have the phase diagrams shown in Figs. 5(a,b). For $U = 3$ the on-site repulsion is small enough that no SDW region appears. The intersite V and electron-phonon interaction range compete to give either CDW or PS. For $U = 8$, PS is replaced by SDW. We can estimate the transition point in the Holstein limit: $V = \frac{1}{2}(U - U_{eff}) = \frac{1}{2}(U - \lambda^2/\omega^2) = 2.0$, which agrees well with the $U = 8$ phase diagram at $\xi = 0$. Despite its simplicity, Fig. 5(b) carries a central message of this paper: reasonable choices of V and U suppress the PS which was noted in the first attempts to simulate momentum dependent electron-phonon couplings.

The behavior at $U = 4$ is considerably more complex and hence worth discussing in more detail. Figure 6(a) indicates a small electron kinetic energy until V exceeds a threshold value. Careful examination of the line shapes for $0.8 \lesssim \xi \lesssim 1.1$ reveals that there are two regimes of large $\mathcal{K}_{el}$. As V is increased initially, $\mathcal{K}_{el}$ increases abruptly in magnitude, and then continues a much slower increase. At a second critical V a kink appears, there is a change in the sign of the slope, and the magnitude of $\mathcal{K}_{el}$ begins to fall. In combination with the behavior of other observables, see below, we interpret this to indicate a PS to SDW to CDW evolution with increasing V for these values of ξ. At larger ξ there is an abrupt jump in $\mathcal{K}_{el}$, but then immediately a decrease in magnitude from the newly large values. For $\xi \leq 0.7$, the absence of small $\mathcal{K}_{el}$ indicates that there is no phase separation region for these values of ξ. These correspond to single PS to CDW, and SDW to CDW transitions, respectively.
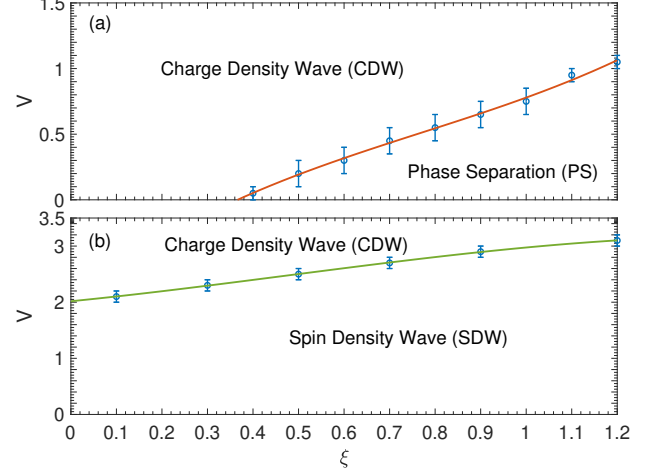

FIG. 5. (Color online) (a) Phase diagram of the HEH model in the V - ξ plane for $U = 3.0$. The on-site repulsion is too weak to produce SDW. (b) Phase diagram of the HEH model in the V - ξ plane for $U = 8.0$. Here the on-site repulsion results in robust SDW phase and the combination of U and V eliminates all phase separation.
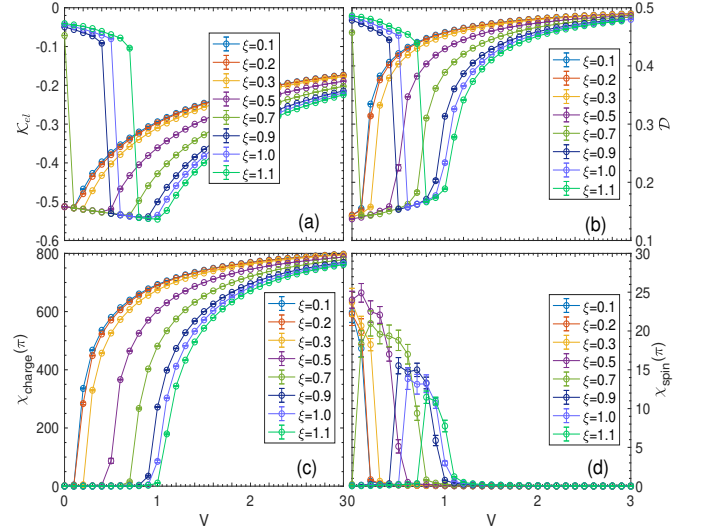

FIG. 6. (Color online) For the HEH model at $U = 4$ and several values of ξ we show as functions of V the (a) electron kinetic energy, (b) the double occupancy, (c) the charge susceptibility, (d) the spin susceptibility. The number of site $N = 32$ and inverse temperature $\beta = 26$. Phonon frequency $\omega = 0.5$ and electron-phonon coupling strength $\lambda_0 = 1.0$.

The the double occupancy curves (Fig. 6(b)) look rather similar to the electron kinetic energy. Here, as discussed earlier, low values of $\mathcal{D}$ are associated with SDW, while large values can be either PS or CDW. The existence of two separate transitions, quite evident in $\mathcal{K}_{el}$ is less clear in $\mathcal{D}$. However, close inspection of the $\xi = 0.9, 1.0$, and 1.1 curves shows that $\mathcal{D}$ increases gradually with V after entering the SDW, but then
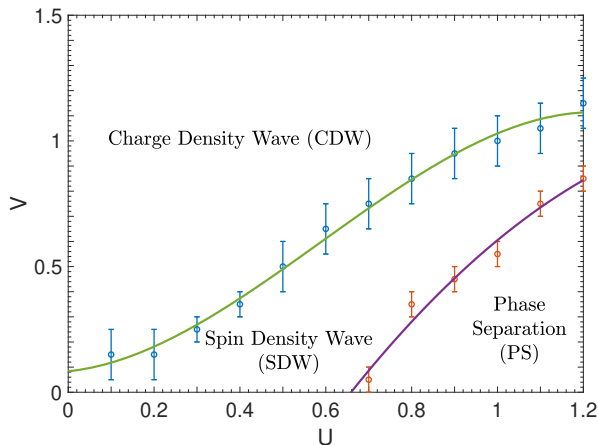
FIG. 7. (Color online) Phase diagram of the HEH model in the $V - \xi$ plane for $U = 4.0$ inferred from Fig. 6. The on-site repulsion is now big enough to give SDW sandwiched in between PS at large ξ and CDW at large V.

abruptly changes slope for yet larger V. This is consistent with changes from PS to SDW to CDW for these ξ.

Figures 6(c) and 6(d) give the evolution of the charge and spin susceptibilities respectively. Consistent with the data from the local observables, χ_{spin} is big only in an intermediate range of V for $\xi \gtrsim 0.7$, below which lies PS and above which CDW. For smaller ξ, SDW phase extends all the way to $V = 1.0$. For all ξ, χ_{charge} grows large above a critical V. The shapes or the curves are not markedly different for $\xi \lesssim 0.7$ where the CDW emerges from SDW, and for $\xi \gtrsim 0.7$ where it emerges from a PS region.

Putting these plots together, we infer the $U = 4$ phase diagram of Fig. 7 which has CDW physics dominant at large V, but two possibilities, SDW and PS, for the nature of the ground state at small V. As with the constant $V = 0.5$ phase diagram of Fig. 3(a) one thus encounters all three ground states as one tunes the value of the electron-electron interactions.

V. 5. CONCLUSIONS

Recent attempts to include momentum dependent (finite range) electron-phonon coupling without electron-electron interactions have concluded that the tendency to phase separation dominates the physics. This is mitigated to some extent[53] by an on-site repulsion U,

nevertheless PS is already dominant beyond relatively small $\xi \gtrsim 0.5$. This puts significant restrictions on the nature of $\lambda(q)$ which would exhibit spatially homogeneous densities- most of the weight would have to be at momenta $q > 2\pi/\xi$, i.e. well outside the first Brillouin Zone.

Here we have introduced a nearest-neighbor Coulomb interaction V to the extended Holstein-Hubbard Hamiltonian and obtained the resulting phase diagrams at half-filling. We have shown even relatively small values of $V \sim \lambda_0$ can stabilize SDW and CDW phases and eliminate (long period) density inhomogeneity. Figure 5(b) is a key result: PS is totally suppressed and the effects of ξ can be discerned in a context of global thermodynamic stability.

Important questions remain open. First, we have not attempted to explore possible metallic phases. These are known to be extremely challenging to address with QMC even in much more simple models, since the gaps can vanish exponentially at weak coupling. Second, we have not doped the system. This paper has exclusively focused on half-filling. CDW and SDW phases tend to be optimized at commensurate filling, but in $d = 1$ the continued presence of Fermi surface nesting can give rise to order at $k < \pi$. We generally expect superconductivity to be aided by some degree of doping; it is already known to exist in models where bond phonons couple to densities on both neighboring sites[26,27]. Much of the existing experimental data on the materials which motivate the study of the model, including some organic superconductors and density wave systems, are away from half-filling. Because the sign problem does not occur at any filling for our model in one dimension, it will be interesting to apply our method to study doped systems. As discussed here at half-filling, a longer-range electron-phonon interaction will play an important role in the competition between phase separation and superconductivity, and we expect this to be the case in the doped system as well.

[1] E. Berger, P. Valášek, and W. von der Linden, Phys. Rev. B **52**, 4806 (1995).

[2] F. F. Assaad and T. C. Lang Phys. Rev. B **76**, 035116 (2007).

[3] E.A. Nowadnick, S. Johnston, B. Moritz, R.T. Scalettar, and T.P. Devereaux, Phys. Rev. Lett. **109**, 246404.

[4] S. Johnston, E.A. Nowadnick, Y.F. Kung, B. Moritz, R.T. Scalettar, and T.P. Devereaux, Phys. Rev. B **87**, 235133

(2013).

[5] S. Yamazaki, S. Hoshino, and Y. Kuramoto, JPS Conf. Proc. **3**, 016021 (2014).

[6] A. Macridin, B. Moritz, M. Jarrell, and T. Maier, J. of Phys.: Cond. Mat. **24**, (2012).

[7] C. B. Mendl, E. A. Nowadnick, E. W. Huang, S. Johnston, B. Moritz, and T. P. Devereaux, Phys. Rev. B **96**, 205141 (2017).

[8] A. Ghosh, S. Kar, and S. Yarlagadda1a, Eur. Phys. J. B **91**, 205 (2018).

[9] S. Karakuzu, L.F. Tocchio, S. Sorella, and F. Becca, Phys. Rev. B **96**, 205145 (2017).

[10] S. Karakuzu and S. Sorella, arXiv:1808.07759.

[11] J. E. Hirsch, R. L. Sugar, D. J. Scalapino, and R. Blankenbecler, Phys. Rev. B **26**, 5033 (1982).

[12] P. Sengupta, A.W. Sandvik, and D.K. Campbell, Phys. Rev. B **65**, 155113 (2002).

[13] M. Nakamura, J. Phys. Soc. Jpn. **68**, 3213 (1999)

[14] M. Nakamura, Phys. Rev. B **61**, 16377 (2000).

[15] A.W. Sandvik, L. Balents, and D.K. Campbell, Phys. Rev. Lett. **92**, 236401 (2004).

[16] M. Tsuchiizu and A. Furusaki, Phys. Rev. Lett. **88**, 056402 (2002).

[17] M. Tsuchiizu and A. Furusaki, Phys. Rev. B **69**, 035103 (2004).

[18] Y. Z. Zhang, Phys. Rev. Lett. **92**, 246404 (2004).

[19] K-M. Tam, S-W. Tsai, and D.K. Campbell, Phys. Rev. Lett. **96**, 036408 (2006).

[20] C. Bourbonnais and D. Jérome, *Physics of Organic Superconductors and Conductors*, A.G. Lebed (ed), Springer, Berlin (2008).

[21] A.J. Berlinsky, Rep. Prog. Phys. **42**, 1243 (1979).

[22] *Density Waves in Solids*, G. Gruner, Taylor and Francis, boca Raton (1994).

[23] R.T. Clay and R.P. Hardikar, Phys. Rev. Lett. **95**, 096401 (2005).

[24] R. P. Hardikar and R. T. Clay, Phys. Rev. B **75**, 245103 (2007).

[25] Ka-Ming Tam, S.-W. Tsai, D. K. Campbell, and A. H. Castro Neto Phys. Rev. B **75**, 161103(R) (2007).

[26] J. Bonča and S.A. Trugman, Phys. Rev. B **64**, 094507 (2001).

[27] K.M. Tam, S.W. Tsai, and D.K. Campbell, Phys. Rev. B **89**, 014513 (2014).

[28] N.C. Costa, T. Blommel, W.-T. Chiu, G.G. Batrouni, and R.T. Scalettar, Phys. Rev. Lett. **120**, 187003 (2018).

[29] E.H. Lieb and F.Y. Wu, Phys. Rev. Lett. **20**, 1445 (1968).

[30] J.E. Hirsch and E. Fradkin, Phys. Rev. B **27**, 4302 (1983).

[31] L.G. Caron and C. Bourbonnais, Phys. Rev. B **29**, 4230 (1984).

[32] D. Schmeltzer, J. Phys. C: Solid State Phys. **20**, 3131 (1987).

[33] C. Bourbonnais and L.G. Caron, J. Phys. (France) **50**, 2751 (1989).

[34] C.Q. Wu, Q.F. Huang, and X. Sun, Phys. Rev. B **52**, R15683 (1995).

[35] Y. Takada, J. Phys. Soc. Japan **65**, 1544 (1996).

[36] T. Hotta and Y. Takada, Physica B **230**, 1037 (1997).

[37] E. Jeckelmann, C. Zhang, and S.R. White, Phys. Rev. B **60**, 7950 (1999).

[38] Y. Takada and A. Chatterjee, Phys. Rev. B **67**, 081102 (2003).

[39] J. Zhao and K. Ueda, J. Phys. Soc. Japan **79**, 074602 (2010).

[40] E. Fehske, A.P. Kampf, M. Sekania, and G. Wellein, Eur. Phys. J. B **31**, 11 (2003).

[41] E. Fehske, G. Wellein, G. Hager, A. Weisse, and A.R. Bishop, Phys. Rev. B **69**, 165115 (2004).

[42] E. Fehske, G. Hager, and E. Jeckelmann, Europhys. Lett. **84**, 57001 (2008).

[43] M. Tezuka, R. Arita, and H. Aoki, Phys. Rev. Lett. **95**, 226401 (2005).

[44] M. Tezuka, R. Arita, and H. Aoki, Phys. Rev. B **76**, 155114 (2007).

[45] S. Ejima and H. Fehske, J. Phys: Conf. Ser. **200**, 012031 (2010)

[46] A. Chatterjee, Adv. Cond. Matt. Phys. 2010, 350787 (2010).

[47] A.S. Alexandrov and B. Ya. Yavidov, Phys. Rev. B **69**, 073101 (2004).

[48] P.E. Spencer, J.H. Samson, P.E. Kornilovitz, and A.S. Alexandrov, Phys. Rev. B **71**, 184310 (2005).

[49] M. Hohenadler, F.F. Assaad, and H. Fehske, Phys. Rev. Lett. **109**, 116407 (2012).

[50] J.P. Hague and P.E. Kornilovitch, Phys. Rev. B **80**, 054301 (2009).

[51] Y. Wang, K. Nakatsukasa, L. Rademaker, T. Berlijn, and S. Johnston, arXiv:1602.00656.

[52] A.G. Swartz, H. Inoue, T.A. Merz, Y. Hikita, S. Raghu, T.P. Devereaux, S. Johnston, and H.Y. Hwang, arXiv:1608.05621.

[53] F. Hébert, B. Xiao, V.G. Rousseau, R.T. Scalettar and G.G. Batrouni, Phys. Rev. B **99**, 075108 (2019).

[54] F. Weber, S. Rosenkranz, J.-P. Castellan, R. Osborn, R. Hott, R. Heid, K.-P. Bohnen, T. Egami, A.H. Said, and D. Reznik, Phys. Rev. Lett. **107**, 107403 (2011).

[55] T.P. Devereaux, A.M. Shvaika, K. Wu, K. Wohlfeld, C.J. Jia, Y. Wang, B. Moritz, L. Chaix, W.-S. Lee, Z.-X. Shen, G. Ghiringhelli, and L. Braicovich, arXiv 1605.03129.

[56] E.Y. Loh, J.E. Gubernatis, R.T. Scalettar, S.R. White, D.J. Scalapino, and R.L. Sugar, Phys. Rev. B **41**, 9301 (1990).

[57] M. Troyer and U-J. Wiese, Phys. Rev. Lett. **94**, 170201 (2005).

[58] G.G. Batrouni, R.T. Scalettar, and G.T. Zimanyi, Phys. Rev. Lett. **65**, 1765 (1990).

[59] N.V. Prokofév, B.V. Svistunov, and I.S. Tupitsyn, Phys. Lett. A **238**, 253 (1998).

[60] V.G. Rousseau, Phys. Rev. E **77**, 056705 (2008).